# OPM-MEG Measuring Phase Synchronization on Source Time Series: Application in Rhythmic Median Nerve Stimulation

Yu-Yu Ma, Yang Gao, Huan-Qi Wu, Xiao-Yu Liang, Yong Li, Hao Lu, Chang-Zeng Liu, and Xiao-Lin Ning

***Abstract*— The magnetoencephalogram (MEG) based on array optically pumped magnetometers (OPMs) has the potential of replacing conventional cryogenic superconducting quantum interference device. Phase synchronization is a common method for measuring brain oscillations and functional connectivity. Verifying the feasibility and fidelity of OPM-MEG in measuring phase synchronization will help its widespread application in the study of aforementioned neural mechanisms. The analysis method on source-level time series can weaken the influence of instantaneous field spread effect. In this paper, the OPM-MEG was used for measuring the evoked responses of 20Hz rhythmic and arrhythmic median nerve stimulation, and the inter-trial phase synchronization (ITPS) and inter-reginal phase synchronization (IRPS) of primary somatosensory cortex (SI) and secondary somatosensory cortex (SII) were analysed. The results find that under rhythmic condition, the evoked responses of SI and SII show continuous oscillations and the effect of resetting phase. The values of ITPS and IRPS significantly increase at the stimulation frequency of 20Hz and its harmonic of 40Hz, whereas the arrhythmic stimulation does not exhibit this phenomenon. Moreover, in the initial stage of stimulation, the ITPS and IRPS values are significantly higher at Mu rhythm in the rhythmic condition compared to arrhythmic. In conclusion, the results demonstrate the ability of OPM-MEG in measuring phase pattern and functional connectivity on source-level, and may also prove beneficial for the study on the mechanism of rhythmic stimulation therapy for rehabilitation.**

***Index Terms*— OPM-MEG, source time series, inter-trial phase synchronization, inter-reginal phase synchronization, functional connectivity, rhythmic stimulation.**

Manuscript received 7 January 2024; revised 27 February 2024; accepted 20 March 2024. Date of publication 26 March 2024; date of current version 1 April 2024. This work was supported in part by the Key Research and Development Program of Shandong Province under Grant 2022ZLGX03 and in part by the Industrial Technology Basic Public Service Platform Project of China under Grant 2022189181. *(Corresponding author: Xiao-Lin Ning.)*

This work involved human subjects or animals in its research. Approval of all ethical and experimental procedures and protocols was granted by the Research Ethics Committee of Beihang University.

Yu-Yu Ma, Huan-Qi Wu, Xiao-Yu Liang, Yong Li, Hao Lu, and Chang-Zeng Liu are with the School of Instrumentation and Optoelectronic Engineering, Beihang University, Beijing 100191, China (e-mail: ma_yuyu@buaa.edu.cn).

Yang Gao and Xiao-Lin Ning are with the School of Instrumentation and Optoelectronic Engineering and the Key Laboratory of Ultra-Weak Magnetic Field Measurement Technology, Ministry of Education, Beihang University, Beijing 100191, China, also with the National Institute of Extremely-Weak Magnetic Field Infrastructure, Hangzhou 310051, China, and also with the National Medicine-Engineering Interdisciplinary Industry-Education Integration Innovation Platform, Shandong Key Laboratory for Magnetic Field-Free Medicine and Functional Imaging, Research Institute of Shandong University, Shandong University, Jinan 250014, China (e-mail: yanggao@buaa.edu.cn; ningxiaolin@buaa.edu.cn).

This article has supplementary downloadable material available at https://doi.org/10.1109/TNSRE.2024.3381173, provided by the authors.

Digital Object Identifier 10.1109/TNSRE.2024.3381173

## I. Introduction

MAGNETOENCEPHALOGRAPHY (MEG) is a non-invasive method for assessing brain function [1], which records the magnetic field signals converted from cortical neuronal electrical activities with millimeter spatial resolution and millisecond temporal resolution [2], [3]. Traditionally, the superconducting quantum interference device (SQUID) is used for detecting the magnetic fields at the fT level on brain. However, SQUID-MEG requires complex and massive ancillary system to maintain its operation at cryogenic liquid helium environment, meanwhile a thick Dewar is required for isolating from low temperature. In this case, the distance between the cryogenic sensors and the scalp is increased and the applicability to head shape is reduced, which result in the decrease of signal amplitude and the accuracy of source reconstruction. In recent years, the optically pumped magnetometers (OPMs) [4], [5] have been offered the measurement of brain magnetic field. With the advantages in compact size, normal temperature operation, and easy configuration specific sensor layout close to the target brain regions for more precise measurement [6], [7], OPM-MEG can obtain higher signal amplitude, reconstruction accuracy, spatial resolution than SQUID-MEG [8], [9], and has the potential of measuring a wider range of disease entities and special populations such as infants [5], [10]. However, OPM-MEG is a new technology in its early stage and the accuracy of its measurement in important neural signal features such as phase synchronization needs to be demonstrated before it can be widely applied in clinical medicine and neuroscience research.

Oscillatory synchronization is commonly present in neural signals [11], [12]. Relative to asynchronous period, the

neurons that oscillate in synchrony are able to consistently exchange bursts of action potentials during the depolarized phase [13], [14], [15], which contributes to the instant communication of dynamic functional networks between brain regions [16]. Recent works reveal that phase pattern can carry more physiological information to a greater degree than amplitude in the measurement of oscillation [17]. Phase synchronization measures the correlation relationship of the phase pattern at a specific frequency during oscillation process. One manner in which phase synchronization can be applied is inter-trial phase synchronization (ITPS). ITPS measures the consistency of signal phase across trials related to a specific event of interest especially in task paradigm [18], [19]. The neural processes, such as auditory and visual perception [20], [21], attention [22], and memory [23], have all been shown to be accompanied by the changes of ITPS values in relevant brain regions.

On the other hand, the dependency between the phases of oscillation signals implies the synchronization relationship between activation and deactivation cycles of neuronal groups [24]. This inter-reginal phase synchronization (IRPS) can be considered as an indication of functional connectivity [18], [25] and provides an important pathway for understanding the integration and dynamic processes of neural mechanisms [26], [27]. More importantly, the disruption of normal rhythmic connectivity is responsible for a large number of neuropathy and psychopathy diseases. Various pathological conditions, including schizophrenia [28], autism spectrum disorder [29], Parkinson [30], Alzheimer's disease [31], epilepsy [32] and so on, are related to the disturbances of the IRPS values.

Generally, phase synchronization can be measured by sensor signals and source time series. The calculation method of using sensor signals is susceptible to the effect of instantaneous field spread, and may lead to inaccurate estimation especially for IRPS. The measurement using source time series directly estimates the neural source activity that generates sensors' signals, which reduces the influence of field spread [33], [34] and has become an increasingly popular tool. To the best of the author's knowledge, the measurement of ITPS and IRPS on source-level is still blank for OPM-MEG. However, verifying the accuracy of the source-level phase synchronization using OPM-MEG is not easy. The correlation relationship between brain regions measured by OPM-MEG still exhibits a low degree of similarity compared with SQUID-MEG even for a same subject in task state paradigm [35]. Therefore, this paper seeks for a study that the measurement of phase synchronization is consistent with the relatively clear brain response, while also can be self-certified the fidelity.

It is proven that the rhythmic stimulation could induce the synchronous oscillation [36], and has widely used for the rehabilitation treatment on the diseases, such as tic disorder [37]. In this paper, the OPM-MEG was applied to measure the oscillation activity induced by the 20Hz rhythmic median nerve stimulation, then the time series of somatosensory cortex contralateral to stimulation after source reconstruction were extracted and used for the analysis of ITPS and IRPS. The results were compared with those of arrhythmic median nerve stimulation.

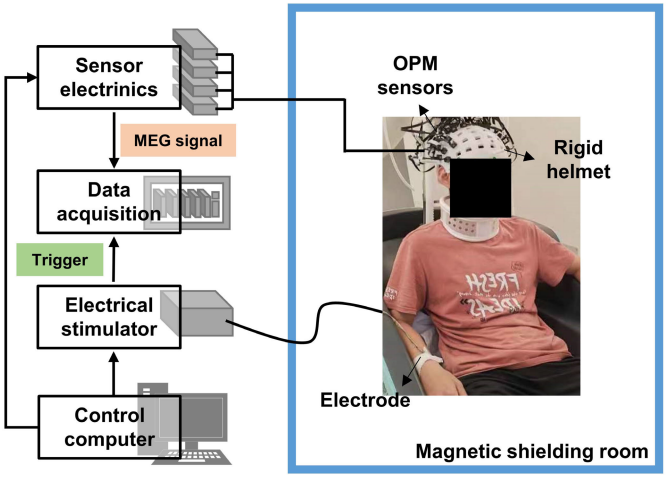


Fig. 1. OPM-MEG system.

## II. Materials and Methods

### A. Subjects

7 healthy subjects (aged 26.7 ± 1.8 years, 6 males and 1 female) participated in the experiment. The subjects are native Chinese speakers, right-handed, and with no known history of congenital developmental diseases, dysaudia, neurological or mental disorders. All subjects had received the informed consent and agreed to participate in the experiment. This study was approved by the Research Ethics Committee of Beihang University.

### B. OPM-MEG System

The OPM-MEG experimental system used in this paper is shown in Fig.1. In this system, OPM sensors (QuSpin Inc., US) were selected for measuring the brain magnetic field signals in the radial direction and placed in magnetically shielded room (MSR). The 3D printed rigid helmet was used for fixing and arranging the OPM sensors. The sensor electronics were monitored the operating status by control computer, and placed outside the MSR for avoiding electromagnetic interference. The MSR provides a remnant magnetic field magnitude $<$ 5nT. The output MEG signals of each OPM sensors were recorded by the data acquisition device (ART technology Inc., China), and the sampling frequency was set to 1 kHz. The releases of median nerve stimulation were controlled by Psychtoolbox software installed in the control computer, and the stimulation was provided by the DS7A commercial electrical stimulator (Digitimer Inc., United Kingdom). Then the trigger signals generated by electrical stimulator were recorded synchronously by the data acquisition device.

### C. Experimental Paradigm

The experimental paradigm of the rhythmic and arrhythmic median nerve electrical stimulation [38], [39] is shown in Fig.2. In the experiment, 28 channels OPM sensors were

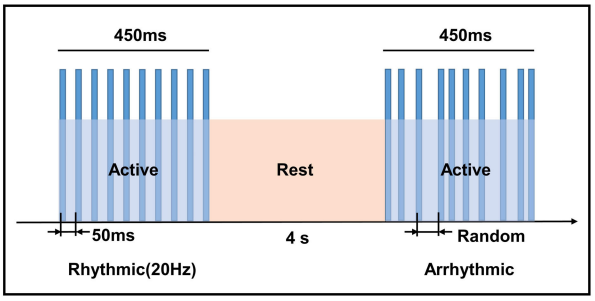


Fig. 2. Experimental paradigm.

selected and fixed in rigid helmet, and its layout covers the somatosensory cortex. The subjects sat on a non-magnetic chair in MSR, hands were kept still using the armrest of chair and ensuring the muscles were relaxed. Stimulation was delivered with bipolar electrodes positioned on the right wrist over the median nerve. The stimulation current was square wave with 0.2ms duration. The simulation location and intensity were individually customized, and can be determined when the subject's thumb had slight twitches. A total of 150 trials were delivered to the median nerve, which include 75 rhythmic trials and 75 arrhythmic trials. Whether the trial was rhythmic or arrhythmic stimulation was random. Each trial consisted of 10 pulses. In rhythmic trials, the inter-pulses interval is 50ms, that is, the stimulation frequency is 20Hz. In arrhythmic trials, the inter-pulses interval is random. But the 10 pulses contained in each trial were all released within 450ms both in rhythmic trials and arrhythmic trials, and the first pulse was always delivered at time 0 and the last pulse was always delivered at 450ms. Then 4s of rest was followed after each trial. In addition, the order of the 150 trials was random and different for every subject.

### D. Preprocessing

The data analysis process is shown in Fig.3. As shown in Fig.3(A), the OPM-MEG data were filtered between 3-48Hz using an overlap-add finite impulse response filter. the phase mode of the filter is 'zero-double', that is, the filter was applied twice to MEG data, once forward, and once backward. The Hamming window is used in the filter and the passband ripple is 0.0194dB, the stopband attenuation is 53 dB. After that, the bad segments were identified and eliminated manually. Then, the homogeneous field correction was used for reducing the interference across the frequency spectrum. Furthermore, the independent component analysis was applied to remove the artifacts such as heartbeat, blinking and so on. Following, the continuous data was segmented into epochs, and each single trial in epochs starts 1.0s before stimulation and ends 2.0s after stimulation. The trials' length was 3.0s.

### E. Coregistration and Source Localization

A structured-light scanner (SHINING 3D Inc., China) was applied to record the 3D digitisations of each subject's head wearing helmet. The anatomical structure with 1.0mm$^3$ spatial resolution was obtained through the anatomical magnetic resonance imaging. Then the OMMR toolbox [40] was used

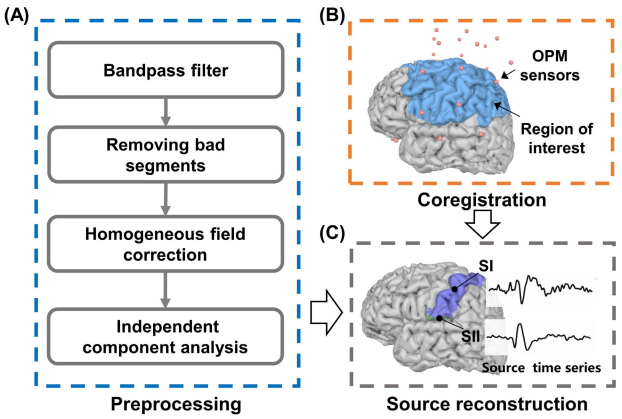


Fig. 3. The schematic diagram of OPM-MEG data analysis process (A) preprocessing; (B) coregistration; (C) source reconstruction and time series extraction.

for coregistration between the 3D digitisations and anatomical structure. Finally, the positions and directions of the OPM sensors relative to brain were obtained, as shown in Fig.3(B).

Freesurfer [41] was used for the cortical reconstruction of subjects' T1 images and then the watershed algorithm was applied to the separation of scalp and skull. The forward solution was computed using single-compartment boundary-element model. The noise covariance matrix was estimated from the baseline data before stimulation (-1.0-0.0s). Then the source distribution was estimated using the dSPM method [42] and the depth weighting was set to 0.8 in order to compensate the bias of the minimum norm estimates towards superficial current [43]. The regularization parameter was set as $1/\mathrm{SNR}^2$. Considering the low signal-to-noise ratio when using single trial for source localization in the following calculations, the SNR was set to 1 consistently. In this paper, the source space was restricted in the region of interest covered by the OPM sensors [44] (blue area in Fig.3(B)). In order to facilitate the comparison of source distribution between rhythmic and arrhythmic stimulation, the cortical surface of every subject mapped to the "fsaverage" template [45]. Those calculations were implemented in MNE-Python [46], [47].

### F. SEFs Extraction

In general, unilateral median nerve somatosensory stimulation will induce somatosensory evoked magnetic fields (SEFs) and activate the primary somatosensory cortex (SI) and secondary somatosensory cortex (SII) [48]. Therefore, the following source-level analyses were conducted on the SI and SII regions contralateral to the stimulation. The SI region is located in the postcentral gyrus and consists of the brain regions of 1, 2, and 3 in the Brodmann atlas [49]. The SII region is a part of the parietal operculum and situated in the upper bank of Sylvian fissure [50], [51], and the region 43 in the Brodmann atlas was selected as the calculation region for SII [52]. The positions of the SI and SII region are shown in Fig.3(C).

In order to investigate the brain activity measured by OPM-MEG, the superposed average method was applied to

the epochs data, then the SEFs of SI and SII regions at 3-48Hz broadband were extracted after source localization. To determine whether 20Hz rhythmic stimulation induces oscillatory synchronization, the preprocessed data was filtered between 15-25Hz broadband (center frequency is 20Hz for the 20 Hz stimulation). After superposed average and source localization, the SEFs related to each pulse were extracted for analysis.

### G. ITPS Calculation

The ITPS value was represented as the resulting of complex phase angle of the single-trial time series in SI and SII regions after source localization, using the following equation [53]:

$$\mathrm{ITPS}^{t,f} = \left| \frac{1}{N} \sum_{n=1}^{N} e^{i\phi^{t,f}} \right|. \tag{1}$$

where $N$ is the number of trials, $\phi^{t,f}$ is the phase angle in radians of the datapoint at trial $n$, frequency $f$ and time $t$. In calculation, the phase angle was given by the Morlet wavelet transform in the range of 5-45Hz, and the frequency resolution was 1Hz. Then the ITPS values were normalized by subtracting the mean of baseline values followed by dividing by the mean of baseline values. The result is a value between 0 and 1 with close to 1 reflecting greater consistency across trials, whereas a lower value indicating high variability between trials.

### H. IRPS Calculation

IRPS was also calculated in the single-trial data, and quantified by the average of the phase angle differences between the source time series of SI and SII regions. The IRPS measure was formalized in the following equation [54]:

$$\mathrm{IRPS}^{t,f} = \left| \frac{1}{N} \sum_{n=1}^{N} e^{i(\phi_{SI}^{t,f} - \phi_{SII}^{t,f})} \right|. \tag{2}$$

where $N$ is the number of trials, $\phi_{SI}^{t,f}$, $\phi_{SII}^{t,f}$ designate the phase angle of the source time series in SI and SII at the trial $n$, frequency $f$ and time $t$ respectively. The phase angle used in IRPS calculation was also obtained by Morlet wavelet transform from 5 to 45 Hz, with the frequency resolution of 1Hz. If the signals of the two brain regions fluctuate synchronously over time, the difference in their phase angles will be constant, producing the IRPS value close to 1. On the contrary, if two source time series fluctuate randomly over time, the changes of phase angles differences will be significant, resulting in the IRPL value close to 0.

### I. Statistical Analysis

In this paper, the Wilcoxon signed rank test was used for the statistically compare of SEFs at each timepoint in the stimulation stage (0-0.5s after stimulation). What's more, a bootstrapping method [55], [56] was adopted for testing whether the ITPS and IRPS values of the rhythmic condition were significantly different from those of arrhythmic. Therefore, the investigated population and the reference population

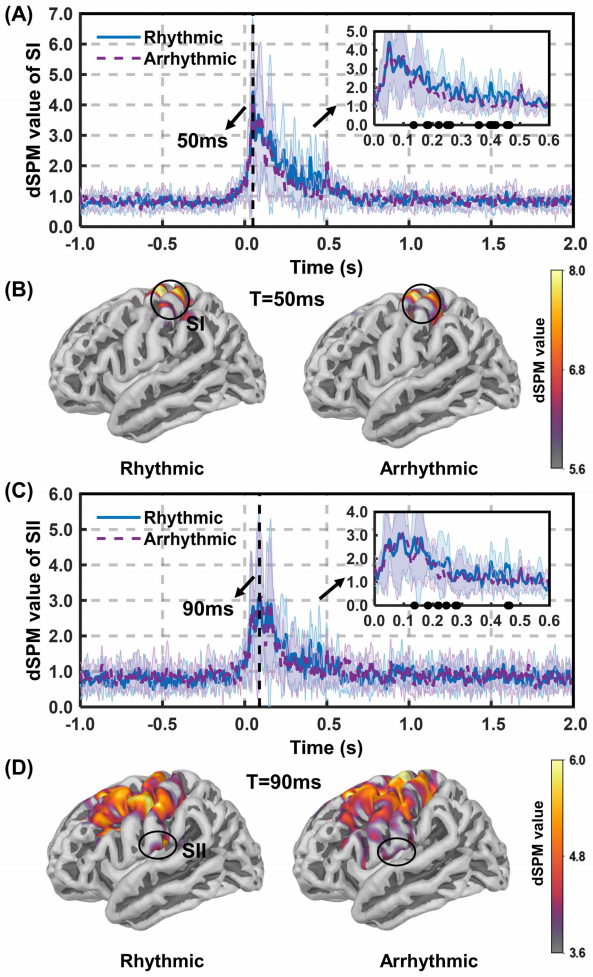


Fig. 4. The evoked responses of somatosensory cortex at 3-48 Hz broadband (A) SEFs of SI region; (B) source activation at peak time of SEFs in SI region; (C) SEFs of SII region; (D) source activation at peak time of SEFs in SII region (the solid line represents the mean and the shaded area represents the standard deviation between subjects in (A) and (C), the black line along the x-axis in the photomicrographs of (A) and (C) marks the timepoints which are significant difference, $p < 0.05$).

were extracted for comparison and they were the collections of the ITPS and IRPS values within the time interval of post stimulation (0.0-2.0s) from each subject in rhythmic and arrhythmic conditions respectively. The null hypothesis is that there is no difference in means between the investigated population and the reference population. Then pseudo-t statistic was constructed as the difference of the mean of the two populations followed by dividing by the pooled variance of the two populations. The significance level (p-values) for the null hypothesis is obtained from the distribution of pseudo-t statistic. In order to address the problem of multiple comparisons, the false discovery rate (FDR) [57] was applied to correct the p-values.

## III. Results

### A. Evoked Response

The evoked responses of SI and SII regions at 3-48Hz broadband in rhythmic and arrhythmic conditions are shown

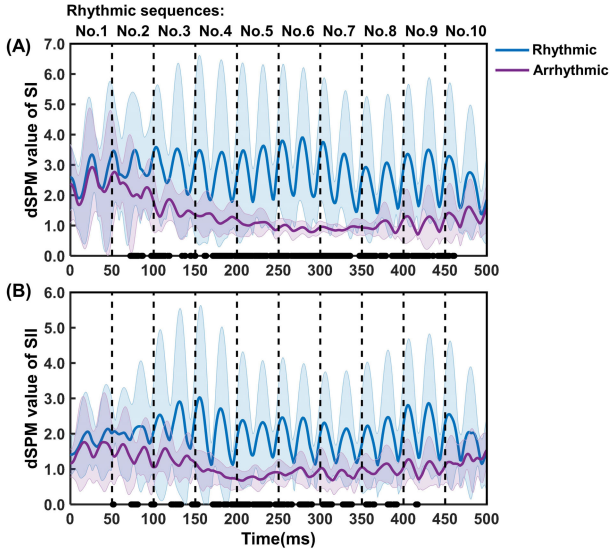


Fig. 5. The evoked responses of the somatosensory cortex at 15-25Hz broadband (A) the evoked response of SI region; (B) the evoked response of SII region (the solid line represents the mean and the shaded area represents the standard deviation, the significantly different timepoints are marked as black line along the x-axis, $p < 0.05$).

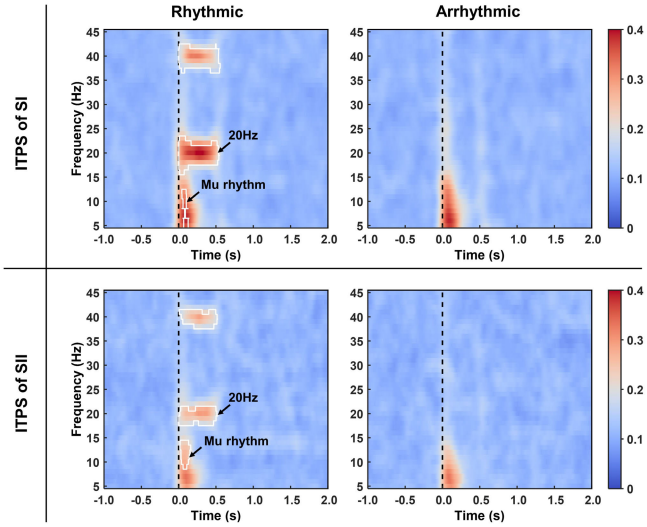


Fig. 6. The averaged ITPS values of SI and SII regions under rhythmic and arrhythmic stimulation conditions (the statistically significant time-frequency points are outlined in white, $p < 0.005$, FDR corrected).

in Fig.4. From the SEFs, it can be seen that the oscillations are exhibited both at the SI and SII regions after rhythmic stimulation. Among them, the maximum value of SEFs in SI region is at about 50ms, and the region of source activation with the max dSPM value is located at postcentral gyrus, which is corresponds to the somatosensory mapping region on brain of right median nerve. While the SII region reaches its maximum value of evoked response at about 90ms and is generated in the superior bank of the Sylvian fissure in the parietal operculum. In addition, the amplitude of the evoked responses in SII region is also smaller than that of SI region.

Fig.5 shows the evoked response of the somatosensory cortex at 15-25 Hz broadband (an example of single subject was provided in supplementary materials). In the initial stage of stimulation, the evoked responses of rhythmic and arrhythmic conditions show similar trends. However, after second pulse, the evoked responses of rhythmic and arrhythmic stimulation show significant differences both in SI and SII regions($p < 0.05$). The SEFs of rhythmic stimulation present sustained oscillations, with a resetting phase after each pulse stimulation, whereas in the arrhythmic stimulation, the amplitude of SEFs reduces gradually, indicating the brain's adaptation to the stimulation. Perhaps because the delivered time of first and last electrical pulse in rhythmic condition is same with arrhythmic, the significantly different timepoints of SEFs in SI and SII are concentrated in the middle segment of the trial.

## B. ITPS Analysis

The averaged ITPS values across subjects of SI and SII regions under the condition of rhythmic and arrhythmic stimulation are shown in Fig.6. Compared with the arrhythmic condition, the significantly increased ITPS values of rhythmic condition are at the time-frequency points which centre on the stimulation frequency of 20Hz as well as its harmonic frequency of 40Hz, and maintain during the time interval of stimulation stage ($p < 0.005$, FDR corrected). In addition, the ITPS values both in rhythmic and arrhythmic conditions present an initial increase across a wide range of frequencies, but the regions where the ITPS values of rhythmic condition significantly higher than arrhythmic are only within the frequency bands of Mu rhythm (6-14Hz) [58] ($p < 0.005$, FDR corrected)

## C. IRPS Analysis

Previous studies have shown that the functional connectivity will be increased at the stimulation frequency [59]. In this paper, the IRPS is used for characterizing the connectivity, and it is expected that the strong phase synchronization will also be presented at the frequency of the stimulation itself (20 Hz). To test this hypothesis, the phase synchronization values between the time series of SI and SII regions are calculated at each frequency point, and the results are shown in Fig.7.

As shown in Fig.7, the phase synchronization between SI and SII regions statistically significantly increases at 20Hz and 40Hz in rhythmic condition compared to that of arrhythmic ($p < 0.005$, FDR corrected). Furthermore, the significantly higher ITPS values at Mu rhythm are also observed in the initial stage of rhythmic stimulation ($p < 0.005$, FDR corrected). The mean and standard deviation of the frequency dependent IRPS values within 0-500ms after stimulation are shown in Fig.8, which indicates the comprehensive constitution of all subjects. The values of phase synchronization of rhythmic condition are higher than those of arrhythmic condition at Mu rhythm, 20Hz, and 40Hz, whereas the curves of IRPS value along with frequency are almost overlap in other broadband, such as 25-35Hz.

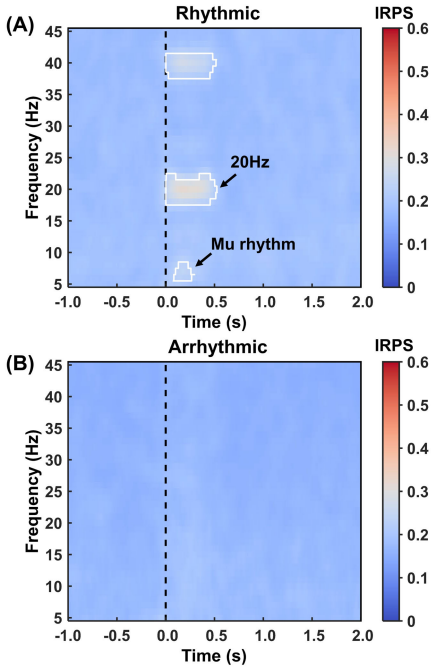


Fig. 7. Phase synchronization between SI and SII regions (A) the averaged IRPS value of rhythmic stimulation; (B) the averaged IRPS value of arrhythmic stimulation (the statistically significant time-frequency points are outlined in white, p< 0.005, FDR corrected).

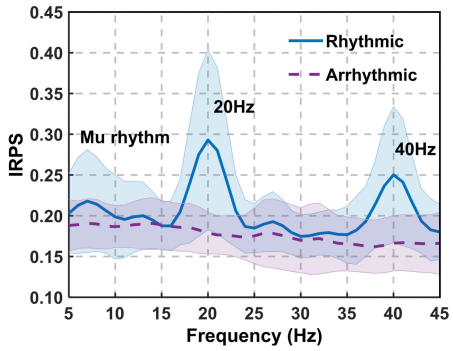


Fig. 8. The variation of IRPS value with frequency within the time range of 0-500ms (the line represents the mean between subjects, and the shaded area represents the standard deviation).

## IV. Discussion

This is the first study to measure the phase synchronization on source-level time series using OPM sensors to the best of author's knowledge. In this paper, the 20Hz rhythmic and arrhythmic median nerve stimulation were measured by the OPM-MEG system. After source reconstruction, the SEFs of SI and SII regions were compared, and then the source time series of single trial were used for the ITPS and IRPS analyses. The results show that under rhythmic condition, the evoked responses in the SI and SII regions present continuous oscillation and effect of resetting phase, the ITPS values significantly increase at the stimulation frequency of 20Hz and harmonic frequency of 40Hz compared to those of arrhythmic condition. It is proved that the fidelity of OPM-MEG in measuring source-level time series and phase consistency for each trial. Moreover, it is found that the IRPS values between SI and SII regions also significantly increases at the stimulation frequency in the rhythmic condition, which demonstrates the feasibility of the OPM-MEG measurement in functional connectivity from the perspective of phase synchronization.

Rhythmic stimulation could prove therapeutically beneficial for the diseases related to hyperexcitability within the sensorimotor cortex, such as Tourette syndrome [39], [60] and the rehabilitation about the body function, such as movement [61], speech and language [62]. Previous studies have shown that rhythmic stimulation, for example transcranial magnetic stimulation [63] and electrical stimulation [38], leads to the synchronization of oscillation response, which includes the characteristics of continuous oscillations, phase resetting in SEFs, and the increased ITPS values at stimulation frequency on somatosensory cortex [38], [64]. The measurement results using OPM-MEG in this paper replicate the aforementioned findings. However, previous researches only discussed the general response of the somatosensory cortex. Oscillatory activity related to the stimulation with certain frequency is not only induced in the primary cortex associated with the sensation, but also transmits to downstream regions in the brain information processing [65], [66]. This paper further marks off the SI and SII regions for the synchronization analysis.

In this paper, the source reconstruction clearly shows that the SI and SII regions are activated both in rhythmic and arrhythmic stimulation and reach their maximum values at bout 50ms and 90ms respectively, reflecting the time course of the somatosensory cortex in processing the stimulation information [67], [68]. At the maximum evoked response in SI region, the source activation is mainly located in the middle of the postcentral gyrus, while at the maximum evoked response of SII region, besides the source activation in the parietal operculum, the activation region at the middle of the postcentral gyrus is also observed, and the two active regions could be separated by the inactive brain regions between them. The results show that 28-channel OPM-MEG which covers the somatosensory cortex can measure source activation precisely. In addition, previous literatures [6], [69] has also demonstrated the feasibility and reliability of source estimation using about 30 OPM sensors with local layout on scalp. However, in this paper or other existing OPM-MEG systems [35], [70], the numbers of sensors are relatively small. In such cases, the source localization may suffer from leakage, which refers to that the nerve activity generated by a particular brain region spreads or leaks to neighboring regions. Due to the ill-posed feature in EEG/MEG inverse problem, source leakage could affect the spatial resolution. Consequently, although the 28-channel OPM-MEG in this paper offers good characterization on source localization, more sources in the brain can enable to resolve and the spatial specificity will be significantly improved with the increase in the number of sensors in the future.

The SEFs of rhythmic and arrhythmic conditions at 15-25 Hz broadband present similarity in the initial stage of stimulation, which is consistent with the evoked response of single electrical stimulation [71]. After the second pulse, the evoked responses show significant differences between rhythmic and arrhythmic conditions. Under rhythmic condition,

the SEFs in the SI and SII regions show relatively complete oscillation cycles, with phase resetting after each pulse stimulation. Whereas in arrhythmic condition, the SEFs do not present the oscillations, and the amplitudes of SEFs also decrease continuously perhaps due to the adaptation of brain to the stimulation. The results show that both SI and SII regions are induced the oscillatory responses by rhythmic stimulation.

When matched with the external stimulation sequences, the oscillation system will generate resonance, and the brain is also such oscillation system. The synchronization phenomena in brain reflects the highly specific neural oscillation, as well as the sequential temporal activity of the neural information processes in response to the incoming sensory stimulation [72]. Compared to arrhythmic condition, the ITPS values of the SI and SII regions in rhythmic condition are significantly increased in stimulation frequency of 20Hz and the harmonics frequency of 40Hz, suggesting that the cortical oscillation synchronizes with the pulses of rhythmic stimulation. The synchronization, also refers to as neural entrainment [73], is considered to be vital for sensory gain [74], [75], cognitive memory [65] and so on.

Synchronization activity between neuron groups, often associated with the communication of functional networks, is considered to provide a method for integrating anatomically distributed processing in the brain [76]. IRPS is the widely used indicator of reflecting the connectivity in brain networks. In this paper, the statistically significant time-frequency points of the phase synchronization between the SI and SII regions with the strongest values are at the stimulation frequency in the rhythmic condition. The phenomenon of increased connectivity at stimulation frequency has been also observed in the former research such as rhythmic vibrotactile [59] and vision stimulation [77], which refers to the entrainment characteristic of ongoing neural oscillations, and is in accordance with the neural mechanism of "communication through coherence" [14], [78]. This also proves the feasibility and rationality of the results of functional connectivity measured by OPM-MEG.

In addition, the ITPS and IRPS values of rhythmic condition in Mu rhythm are significantly higher than those of arrhythmic during the initial stage of stimulation. Mu rhythm is extensively linked to the somatosensory function of brain [79], [80]. The increase of phase synchronization in Mu rhythm may promote the cortical processing of the specific stimulation frequency by improving local and remote interactions of neurons [81].

## V. Conclusion

In this paper, the OPM-MEG system was used for measuring the evoked responses of 20Hz rhythmic and arrhythmic median nerve stimulation. The results find that besides SI region, SII region also presents continuous oscillation and the effect of resetting phase in rhythmic stimulation, which demonstrates the fidelity of the measurement of endogenous oscillation and source time series using OPM-MEG. On this basis, the phase synchronization of SI and SII regions was analyzed, and it is found that under rhythmic condition, the significantly increased values of ITPS and IRPS are at the same frequency with external stimulation. The results add the evidence of the feasibility of OPM-MEG in measuring oscillation synchronization and functional connectivity on source-level, and shed light on the mechanism of rhythmic stimulation in treating the diseases such as tic disorder.

## References


[1] D. O. Cheyne, "MEG studies of sensorimotor rhythms: A review," *Experim. Neurol.*, vol. 245, pp. 27–39, Jul. 2013, doi: 10.1016/j.expneurol.2012.08.030.

[2] A. Jaiswal et al., "Comparison of beamformer implementations for MEG source localization," *NeuroImage*, vol. 216, Aug. 2020, Art. no. 116797, doi: 10.1016/j.neuroimage.2020.116797.

[3] A. Tarkiainen, M. Liljeström, M. Seppä, and R. Salmelin, "The 3D topography of MEG source localization accuracy: Effects of conductor model and noise," *Clin. Neurophysiol.*, vol. 114, no. 10, pp. 1977–1992, Oct. 2003, doi: 10.1016/s1388-2457(03)00195-0.

[4] N. Aslam et al., "Quantum sensors for biomedical applications," *Nature Rev. Phys.*, vol. 5, no. 3, pp. 157–169, Feb. 2023, doi: 10.1038/s42254-023-00558-3.

[5] M. J. Brookes et al., "Magnetoencephalography with optically pumped magnetometers (OPM-MEG): The next generation of functional neuroimaging," *Trends Neurosci.*, vol. 45, no. 8, pp. 621–634, Aug. 2022, doi: 10.1016/j.tins.2022.05.008.

[6] N. An et al., "Imaging somatosensory cortex responses measured by OPM-MEG: Variational free energy-based spatial smoothing estimation approach," *iScience*, vol. 25, no. 2, Feb. 2022, Art. no. 103752, doi: 10.1016/j.isci.2022.103752.

[7] J. Iivanainen, M. Stenroos, and L. Parkkonen, "Measuring MEG closer to the brain: Performance of on-scalp sensor arrays," *NeuroImage*, vol. 147, pp. 542–553, Feb. 2017, doi: 10.1016/j.neuroimage.2016.12.048.

[8] E. Boto et al., "A new generation of magnetoencephalography: Room temperature measurements using optically-pumped magnetometers," *NeuroImage*, vol. 149, pp. 404–414, Apr. 2017, doi: 10.1016/j.neuroimage.2017.01.034.

[9] E. Boto et al., "On the potential of a new generation of magnetometers for MEG: A beamformer simulation study," *PLoS One*, vol. 11, no. 8, Aug. 2016, Art. no. e0157655, doi: 10.1371/journal.pone.0157655.

[10] C. Wang et al., "Methods for improving movement compatibility of wearable OPM-MEG: A review," *IEEE Sensors J.*, vol. 23, no. 24, pp. 30037–30050, Dec. 2023, doi: 10.1109/JSEN.2023.3329043.

[11] G. Buzsáki and A. Draguhn, "Neuronal oscillations in cortical networks," *Science*, vol. 304, no. 5679, pp. 1926–1929, Jun. 2004, doi: 10.1126/science.1099745.

[12] D. Wang, Y. Sun, H. Shi, and F. Wang, "A group analysis of oscillatory phase and phase synchronization in cortical networks," *IEEE Access*, vol. 8, pp. 59182–59199, 2020, doi: 10.1109/ACCESS.2020.2978161.

[13] T. C. Handy, *Brain Signal Analysis: Advances in Neuroelectric and Neuromagnetic Methods*. Cambridge, MA, USA: MIT Press, 2009, pp. 171–204, doi: 10.7551/mitpress/9780262013086.001.0001.

[14] P. Fries, "A mechanism for cognitive dynamics: Neuronal communication through neuronal coherence," *Trends Cognit. Sci.*, vol. 9, no. 10, pp. 474–480, Oct. 2005, doi: 10.1016/j.tics.2005.08.011.

[15] J. Fell and N. Axmacher, "The role of phase synchronization in memory processes," *Nature Rev. Neurosci.*, vol. 12, no. 2, pp. 105–118, Feb. 2011, doi: 10.1038/nrn2979.

[16] P. J. Uhlhaas, C. Haenschel, D. Nikolic, and W. Singer, "The role of oscillations and synchrony in cortical networks and their putative relevance for the pathophysiology of schizophrenia," *Schizophrenia Bull.*, vol. 34, no. 5, pp. 927–943, Jul. 2008, doi: 10.1093/schbul/sbn062.

[17] B. S. W. Ng, N. K. Logothetis, and C. Kayser, "EEG phase patterns reflect the selectivity of neural firing," *Cerebral Cortex*, vol. 23, no. 2, pp. 389–398, Feb. 2013, doi: 10.1093/cercor/bhs031.

[18] S. Morales and M. E. Bowers, "Time-frequency analysis methods and their application in developmental EEG data," *Develop. Cognit. Neurosci.*, vol. 54, Apr. 2022, Art. no. 101067, doi: 10.1016/j.dcn.2022.101067.

[19] V. Mancini et al., "Aberrant developmental patterns of gamma-band response and long-range communication disruption in youths with 22q11.2 deletion syndrome," *Amer. J. Psychiatry*, vol. 179, no. 3, pp. 204–215, Mar. 2022, doi: 10.1176/appi.ajp.2021.21020190.

[20] S. van Noordt, J. A. Desjardins, and M. Elsabbagh, "Inter-trial theta phase consistency during face processing in infants is associated with later emerging autism," *Autism Res.*, vol. 15, no. 5, pp. 834–846, May 2022, doi: 10.1002/aur.2701.

[21] L. Yu, S. Wang, D. Huang, X. Wu, and Y. Zhang, "Role of inter-trial phase coherence in atypical auditory evoked potentials to speech and nonspeech stimuli in children with autism," *Clin. Neurophysiol.*, vol. 129, no. 7, pp. 1374–1382, Jul. 2018, doi: 10.1016/j.clinph.2018.04.599.

[22] B. Zareian, K. Maboudi, M. R. Daliri, H. A. Moghaddam, S. Treue, and M. Esghaei, "Attention strengthens across-trial pre-stimulus phase coherence in visual cortex, enhancing stimulus processing," *Sci. Rep.*, vol. 10, no. 1, p. 4837, Mar. 2020, doi: 10.1038/s41598-020-61359-7.

[23] J. E. Kragel et al., "Hippocampal theta coordinates memory processing during visual exploration," *eLife*, vol. 9, Mar. 2020, Art. no. e52108, doi: 10.7554/elife.52108.

[24] C. Hatlestad-Hall et al., "Reliable evaluation of functional connectivity and graph theory measures in source-level EEG: How many electrodes are enough?" *Clin. Neurophysiol.*, vol. 150, pp. 1–16, Jun. 2023, doi: 10.1016/j.clinph.2023.03.002.

[25] L. Marzetti, A. Basti, F. Chella, A. D'Andrea, J. Syrjälä, and V. Pizzella, "Brain functional connectivity through phase coupling of neuronal oscillations: A perspective from magnetoencephalography," *Frontiers Neurosci.*, vol. 13, p. 964, Sep. 2019, doi: 10.3389/fnins.2019.00964. Accessed: Jan. 5, 2024.

[26] K. J. Friston, "Functional and effective connectivity: A review," *Brain Connectivity*, vol. 1, no. 1, pp. 13–36, Jan. 2011, doi: 10.1089/brain.2011.0008.

[27] F. V. Farahani, W. Karwowski, and N. R. Lighthall, "Application of graph theory for identifying connectivity patterns in human brain networks: A systematic review," *Frontiers Neurosci.*, vol. 13, p. 585, Jun. 2019, doi: 10.3389/fnins.2019.00585.

[28] M. Maran, T. Grent-'t-Jong, and P. J. Uhlhaas, "Electrophysiological insights into connectivity anomalies in schizophrenia: A systematic review," *Neuropsychiatric Electrophysiol.*, vol. 2, no. 1, p. 6, Nov. 2016, doi: 10.1186/s40810-016-0020-5.

[29] J. R. Isler, K. M. Martien, P. G. Grieve, R. I. Stark, and M. R. Herbert, "Reduced functional connectivity in visual evoked potentials in children with autism spectrum disorder," *Clin. Neurophysiol.*, vol. 121, no. 12, Dec. 2010, doi: 10.1016/j.clinph.2010.05.004.

[30] L. di Biase, L. Ricci, M. L. Caminiti, P. M. Pecoraro, S. P. Carbone, and V. Di Lazzaro, "Quantitative high density EEG brain connectivity evaluation in Parkinson's disease: The phase locking value (PLV)," *J. Clin. Med.*, vol. 12, no. 4, p. 1450, Feb. 2023, doi: 10.3390/jcm12041450.

[31] C. T. Briels, D. N. Schoonhoven, C. J. Stam, H. de Waal, P. Scheltens, and A. A. Gouw, "Reproducibility of EEG functional connectivity in Alzheimer's disease," *Alzheimer's Res. Therapy*, vol. 12, no. 1, p. 68, Jun. 2020, doi: 10.1186/s13195-020-00632-3.

[32] J. Cao et al., "Using interictal seizure-free EEG data to recognise patients with epilepsy based on machine learning of brain functional connectivity," *Biomed. Signal Process. Control*, vol. 67, May 2021, Art. no. 102554, doi: 10.1016/j.bspc.2021.102554.

[33] J. M. Schoffelen and J. Gross, "Source connectivity analysis with MEG and EEG," *Human Brain*, vol. 30, no. 6, pp. 1857–1865, Jun. 2009, doi: 10.1002/hbm.20745.

[34] J. M. Palva et al., "Ghost interactions in MEG/EEG source space: A note of caution on inter-areal coupling measures," *NeuroImage*, vol. 173, pp. 632–643, Jun. 2018, doi: 10.1016/j.neuroimage.2018.02.032.

[35] E. Boto et al., "Measuring functional connectivity with wearable MEG," *NeuroImage*, vol. 230, Apr. 2021, Art. no. 117815, doi: 10.1016/j.neuroimage.2021.117815.

[36] G. Thut, C. Miniussi, and J. Gross, "The functional importance of rhythmic activity in the brain," *Current Biol.*, vol. 22, no. 16, pp. 658–663, Aug. 2012, doi: 10.1016/j.cub.2012.06.061.

[37] B. M. Maiquez et al., "A double-blind, sham-controlled, trial of home-administered rhythmic 10-Hz median nerve stimulation for the reduction of tics, and suppression of the urge-to-tic, in individuals with Tourette syndrome and chronic tic disorder," *J. Neuropsychol.*, vol. 17, no. 3, pp. 540–563, Sep. 2023, doi: 10.1111/jnp.12313.

[38] M. S. Houlgreave, B. M. Maiquez, M. J. Brookes, and S. R. Jackson, "The oscillatory effects of rhythmic median nerve stimulation," *NeuroImage*, vol. 251, May 2022, Art. no. 118990, doi: 10.1016/j.neuroimage.2022.118990.

[39] B. M. Maiquez et al., "Entraining movement-related brain oscillations to suppress tics in Tourette syndrome," *Current Biol.*, vol. 30, no. 12, pp. 2334–2342.e3, Jun. 2020, doi: 10.1016/j.cub.2020.04.044.

[40] F. Cao et al., "OMMR: Co-registration toolbox of OPM-MEG and MRI," *Frontiers Neurosci.*, vol. 16, Sep. 2022, Art. no. 984036, doi: 10.3389/fnins.2022.984036.

[41] B. Fischl, "FreeSurfer," *NeuroImage*, vol. 62, no. 2, pp. 774–781, Aug. 2012, doi: 10.1016/j.neuroimage.2012.01.021.

[42] A. M. Dale et al., "Dynamic statistical parametric mapping," *Neuron*, vol. 26, no. 1, pp. 55–67, Apr. 2000, doi: 10.1016/s0896-6273(00)81138-1.

[43] F.-H. Lin, T. Witzel, S. P. Ahlfors, S. M. Stufflebeam, J. W. Belliveau, and M. S. Hämäläinen, "Assessing and improving the spatial accuracy in MEG source localization by depth-weighted minimum-norm estimates," *NeuroImage*, vol. 31, no. 1, pp. 160–171, May 2006, doi: 10.1016/j.neuroimage.2005.11.054.

[44] J. Iivanainen, R. Zetter, and L. Parkkonen, "Potential of on-scalp MEG: Robust detection of human visual gamma-band responses," *Human Brain Mapping*, vol. 41, no. 1, pp. 150–161, Jan. 2020, doi: 10.1002/hbm.24795.

[45] B. Fischl, M. I. Sereno, R. B. Tootell, and A. M. Dale, "High-resolution intersubject averaging and a coordinate system for the cortical surface," *Human Brain Mapping*, vol. 8, no. 4, pp. 272–284, 1999, doi: 10.1002/(SICI)1097-0193(1999)8:43.0.CO;2-4.

[46] A. Gramfort, "MEG and EEG data analysis with MNE-Python," *Frontiers Neurosci.*, vol. 7, p. 267, 2013, doi: 10.3389/fnins.2013.00267. Accessed: Jan. 5, 2024.

[47] A. Gramfort et al., "MNE software for processing MEG and EEG data," *NeuroImage*, vol. 86, pp. 446–460, Feb. 2014, doi: 10.1016/j.neuroimage.2013.10.027.

[48] R. Kakigi, "Somatosensory evoked magnetic fields following median nerve stimulation," *Neurosci. Res.*, vol. 20, no. 2, pp. 165–174, Aug. 1994, doi: 10.1016/0168-0102(94)90034-5.

[49] E. Kropf, S. K. Syan, L. Minuzzi, and B. N. Frey, "From anatomy to function: The role of the somatosensory cortex in emotional regulation," *Brazilian J. Psychiatry*, vol. 41, no. 3, pp. 261–269, May 2019, doi: 10.1590/1516-4446-2018-0183.

[50] J. Ruben, "Somatotopic organization of human secondary somatosensory cortex," *Cerebral Cortex*, vol. 11, no. 5, pp. 463–473, May 2001, doi: 10.1093/cercor/11.5.463.

[51] R. V. Bretas, M. Taoka, H. Suzuki, and A. Iriki, "Secondary somatosensory cortex of primates: Beyond body maps, toward conscious self-in-the-world maps," *Exp. Brain Res.*, vol. 238, no. 2, pp. 259–272, Feb. 2020, doi: 10.1007/s00221-020-05727-9.

[52] L. Moreno-López, C. Soriano-Mas, E. Delgado-Rico, J. S. Rio-Valle, and A. Verdejo-García, "Brain structural correlates of reward sensitivity and impulsivity in adolescents with normal and excess weight," *PLoS One*, vol. 7, no. 11, Nov. 2012, Art. no. e49185, doi: 10.1371/journal.pone.0049185.

[53] M. Jensen, R. Hyder, B. U. Westner, A. Højlund, and Y. Shtyrov, "Speech comprehension across time, space, frequency, and age: MEG-MVPA classification of intertrial phase coherence," *Neuropsychologia*, vol. 188, Sep. 2023, Art. no. 108602, doi: 10.1016/j.neuropsychologia.2023.108602.

[54] J. P. Lachaux, E. Rodriguez, J. Martinerie, and F. J. Varela, "Measuring phase synchrony in brain signals," *Hum. Brain Mapping*, vol. 8, no. 4, pp. 194–208, Jan. 1999, doi: 10.1002/(sici)1097-0193(1999)8:4<194:aid-hbm4>3.0.co;2-c.

[55] P. J. Durka, J. Zygierewicz, H. Klekowicz, J. Ginter, and K. J. Blinowska, "On the statistical significance of event-related EEG desynchronization and synchronization in the time-frequency plane," *IEEE Trans. Biomed. Eng.*, vol. 51, no. 7, pp. 1167–1175, Jul. 2004, doi: 10.1109/TBME.2004.827341.

[56] L. Hu, Z. G. Zhang, and Y. Hu, "A time-varying source connectivity approach to reveal human somatosensory information processing," *NeuroImage*, vol. 62, no. 1, pp. 217–228, Aug. 2012, doi: 10.1016/j.neuroimage.2012.03.094.

[57] Y. Benjamini and D. Yekutieli, "The control of the false discovery rate in multiple testing under dependency," *Ann. Statist.*, vol. 29, no. 4, pp. 1165–1188, Aug. 2001, doi: 10.1214/aos/1013699998.

[58] Y. Wang, K. C. Veluvolu, J.-H. Cho, and M. Defoort, "Adaptive estimation of EEG for subject-specific reactive band identification and improved ERD detection," *Neurosci. Lett.*, vol. 528, no. 2, pp. 137–142, Oct. 2012, doi: 10.1016/j.neulet.2012.09.001.

[59] S. Khan et al., "Somatosensory cortex functional connectivity abnormalities in autism show opposite trends, depending on direction and spatial scale," *Brain*, vol. 138, no. 5, pp. 1394–1409, May 2015, doi: 10.1093/brain/awv043.

[60] A. M. Iverson et al., "Median nerve stimulation for treatment of tics: Randomized, controlled, crossover trial," *J. Clin. Med.*, vol. 12, no. 7, p. 2514, Mar. 2023, doi: 10.3390/jcm12072514.

[61] M. H. Thaut and M. Abiru, "Rhythmic auditory stimulation in rehabilitation of movement disorders: A review of current research," *Music Perception*, vol. 27, no. 4, pp. 263–269, Apr. 2010, doi: 10.1525/mp.2010.27.4.263.

[62] S. Fujii and C. Y. Wan, "The role of rhythm in speech and language rehabilitation: The SEP hypothesis," *Frontiers Human Neurosci.*, vol. 8, p. 777, Oct. 2014, doi: 10.3389/fnhum.2014.00777.

[63] G. Thut, D. Veniero, V. Romei, C. Miniussi, P. Schyns, and J. Gross, "Rhythmic TMS causes local entrainment of natural oscillatory signatures," *Current Biol.*, vol. 21, no. 14, pp. 1176–1185, Jul. 2011, doi: 10.1016/j.cub.2011.05.049.

[64] B. M. Maiquez, G. M. Jackson, and S. R. Jackson, "Entraining movement-related brain oscillations using rhythmic median nerve stimulation," *bioRxiv*, Apr. 2020, doi: 10.1101/2020.03.30.016097.

[65] S. Hanslmayr, N. Axmacher, and C. S. Inman, "Modulating human memory via entrainment of brain oscillations," *Trends Neurosciences*, vol. 42, no. 7, pp. 485–499, Jul. 2019, doi: 10.1016/j.tins.2019.04.004.

[66] H. F. Iaccarino et al., "Gamma frequency entrainment attenuates amyloid load and modifies microglia," *Nature*, vol. 540, no. 7632, pp. 230–235, Dec. 2016, doi: 10.1038/nature20587.

[67] S. F. Worthen, A. R. Hobson, S. D. Hall, Q. Aziz, and P. L. Furlong, "Primary and secondary somatosensory cortex responses to anticipation and pain: A magnetoencephalography study," *Eur. J. Neurosci.*, vol. 33, no. 5, pp. 946–959, Mar. 2011, doi: 10.1111/j.1460-9568.2010.07575.x.

[68] L. Tamè et al., "The contribution of primary and secondary somatosensory cortices to the representation of body parts and body sides: An fMRI adaptation study," *J. Cognit. Neurosci.*, vol. 24, no. 12, pp. 2306–2320, Dec. 2012, doi: 10.1162/jocn_a_00272.

[69] N. An et al., "Multiple source detection based on spatial clustering and its applications on wearable OPM-MEG," *IEEE Trans. Biomed. Eng.*, vol. 69, no. 10, pp. 3131–3141, Oct. 2022, doi: 10.1109/TBME.2022.3161830.

[70] J. Iivanainen et al., "Single-trial classification of evoked responses to auditory tones using OPM- and SQUID-MEG," *J. Neural Eng.*, vol. 20, no. 5, Oct. 2023, Art. no. 056032, doi: 10.1088/1741-2552/acfcd9.

[71] G. Huang and A. Mouraux, "MEP latencies predict the neuromodulatory effect of cTBS delivered to the ipsilateral and contralateral sensorimotor cortex," *PLoS One*, vol. 10, no. 8, Aug. 2015, Art. no. e0133893, doi: 10.1371/journal.pone.0133893.

[72] P. Sauseng and W. Klimesch, "What does phase information of oscillatory brain activity tell us about cognitive processes?" *Neurosci. Biobehavioral Rev.*, vol. 32, no. 5, pp. 1001–1013, Jul. 2008, doi: 10.1016/j.neubiorev.2008.03.014.

[73] Y. Cabral-Calderin and M. J. Henry, "Reliability of neural entrainment in the human auditory system," *J. Neurosci.*, vol. 42, no. 5, pp. 894–908, Feb. 2022, doi: 10.1523/jneurosci.0514-21.2021.

[74] J. Obleser and C. Kayser, "Neural entrainment and attentional selection in the listening brain," *Trends Cognit. Sci.*, vol. 23, no. 11, pp. 913–926, Nov. 2019, doi: 10.1016/j.tics.2019.08.004.

[75] P. Lakatos, G. Karmos, A. D. Mehta, I. Ulbert, and C. E. Schroeder, "Entrainment of neuronal oscillations as a mechanism of attentional selection," *Science*, vol. 320, no. 5872, pp. 110–113, Apr. 5872, doi: 10.1126/science.1154735.

[76] J. M. Palva, S. Palva, and K. Kaila, "Phase synchrony among neuronal oscillations in the human cortex," *J. Neurosci.*, vol. 25, no. 15, pp. 3962–3972, Apr. 2005, doi: 10.1523/JNEUROSCI.4250-04.2005.

[77] C. Jaeger et al., "Targeted rhythmic visual stimulation at individual participants' intrinsic alpha frequency causes selective increase of occipitoparietal BOLD-fMRI and EEG functional connectivity," *NeuroImage*, vol. 270, Apr. 2023, Art. no. 119981, doi: 10.1016/j.neuroimage.2023.119981.

[78] P. Fries, "Rhythms for cognition: Communication through coherence," *Neuron*, vol. 88, no. 1, pp. 220–235, Oct. 2015, doi: 10.1016/j.neuron.2015.09.034.

[79] R. Hari, R. Salmelin, J. P. Mäkelä, S. Salenius, and M. Helle, "Magnetoencephalographic cortical rhythms," *Int. J. Psychophysiol.*, vol. 26, nos. 1–3, pp. 51–62, Jun. 1997, doi: 10.1016/s0167-8760(97)00755-1.

[80] W. A. MacKay, "Synchronized neuronal oscillations and their role in motor processes," *Trends Cognit. Sci.*, vol. 1, no. 5, pp. 176–183, Aug. 1997, doi: 10.1016/s1364-6613(97)01059-0.

[81] M. Sabate, C. Llanos, E. Enriquez, and M. Rodriguez, "Mu rhythm, visual processing and motor control," *Clin. Neurophysiol.*, vol. 123, no. 3, pp. 550–557, Mar. 2012, doi: 10.1016/j.clinph.2011.07.034.